



## Dynamics of plate bending at the trench and slab-plate coupling

**F. A. Capitanio**

*School of Mathematical Sciences and School of Geosciences, Monash University, Clayton, Victoria 3800, Australia  
(fabio.capitanio@sci.monash.edu.au)*

**G. Morra**

*Institute of Geophysics, ETH Zurich, CH-8093 Zurich, Switzerland*

*Also at Dipartimento di Scienze Geologiche, Università Roma Tre, I-00156 Rome, Italy*

**S. Goes**

*Department of Earth Science and Engineering, Imperial College London, London SW7 2AZ, UK*

[1] The bending strength of subducting lithosphere plays a critical role in the Earth's plate tectonics and mantle convection, modulating the amount of slab pull transmitted to the surface and setting the boundary conditions under which plates move and deform. However, it is the subject of a lively debate how much of the potential energy of the downgoing plate is consumed in bending the plate and how the lithospheric strength is defined during this process. We model the subduction of a viscoelastic lithosphere, driven solely by the downgoing plate's buoyancy, freely sinking in a passive mantle, represented by drag forces. To investigate the dynamics of bending, (1) we vary the density and the viscosity profile within the plate from isoviscous, where strength is distributed, to strongly layered, where strength is concentrated in a thin core, and (2) we map the stress, strain, and dissipation along the downgoing plate. The effective plate strength during bending is not a simple function of average plate viscosity but is affected by rheological layering and plate thinning. Earth-like layered plates allow for the transmission of large fractions of slab pull ( $\sim 75\text{--}80\%$ ) through the bend and yield a net slab pull of  $F_{\text{SP}}^{\text{net}} = 1 \text{ to } 6 \times 10^{12} \text{ N m}^{-1}$ , which varies with the buoyancy of plates. In all models, only a minor portion of the energy is dissipated in the bending. Surprisingly, bending dissipation hardly varies with lithospheric viscosity because in our dynamic system, the plates minimize overall dissipation rate by adjusting their bending curvature. As a result, bending dissipation,  $\Phi_{\text{B}}$ , is mainly controlled by the bending moment work rate exerted by slab pull. We propose a new analytical formulation that includes a viscosity-dependent bending radius, which allows for assessment of the relative bending dissipation in the Earth's subduction zones using parameters from a recent global compilation. This yields estimates of  $\Phi_{\text{B}}/\Phi_{\text{TOT}} < 20\%$ . These results suggest that plates on Earth weakly resist bending, yet are able to propagate a large amount of slab pull.

**Components:** 9482 words, 10 figures, 1 table.

**Keywords:** subduction; bending; slab pull; dissipation.

**Index Terms:** 8138 Tectonophysics: Lithospheric flexure; 8104 Tectonophysics: Continental margins: convergent; 8122 Tectonophysics: Dynamics: gravity and tectonics.



Received 1 December 2008; Revised 20 February 2009; Accepted 24 February 2009; Published 1 April 2009.

Capitanio, F. A., G. Morra, and S. Goes (2009), Dynamics of plate bending at the trench and slab-plate coupling, *Geochem. Geophys. Geosyst.*, 10, Q04002, doi:10.1029/2008GC002348.

## 1. Introduction

[2] The downward pull of slabs in the Earth's mantle is the largest force in plate tectonics [Chapple and Tullis, 1977; Forsyth and Uyeda, 1975], driving surface plate motions and deformation. Forces generated by the interaction of sinking slabs and resisting mantle are transferred to the surface through mantle viscous tractions [Becker and O'Connell, 2001; Lithgow-Bertelloni and Richards, 1995, 1998] and directly to the plate through the bending margins [Buffett, 2006; Conrad and Lithgow-Bertelloni, 2002, 2004]. However, little agreement has been achieved on which provides the dominant force. Mantle convection models can provide a good match to plate motions and stress fields [Becker and O'Connell, 2001; Lithgow-Bertelloni and Guynn, 2004; Steinberger et al., 2001]. However, the set of plates boundary forces required is not unique, leaving how the contributions of in-plane forces and mantle drag are partitioned undetermined.

[3] One of the main problems in estimating pull propagation lies in the difficulty of assessing lithospheric properties during bending, as direct access to these regions on Earth is impossible. Several models proposed that partial to complete loss of strength at bending [Di Giuseppe et al., 2008; Stegman et al., 2006] might be responsible for uncoupling the slab and plate [Billen and Gurnis, 2005; Billen and Hirt, 2007; Enns et al., 2005], and could eventually halt subduction [Conrad and Hager, 2001]. However, published subduction models give bending dissipation estimates ranging from as large as 80–90% [Becker et al., 1999; Bellahsen et al., 2005], to 35–50% [Di Giuseppe et al., 2008], to as low as 10–20% [Capitanio et al., 2007; Stegman et al., 2006; Wu et al., 2008].

[4] On the other hand, global flow models show that effective transmission of slab pull, often > 70%, is required to match global plate velocities [Conrad and Lithgow-Bertelloni, 2002, 2004]. Therefore, the global model predictions are in disagreement with a loss of lithospheric strength, requiring plates that bend easily into the mantle, while able to propagate sensitive portions of slab pull.

[5] Geoid observations [Mitrovica, 1996; Moresi and Gurnis, 1996; Zhong and Davies, 1999] and subduction models [Funicello et al., 2008; Schellart, 2008; Wu et al., 2008] constrained the effective viscosity of the plate to be ~100–500 times larger than mantle. Subduction models with this viscosity contrast are relatively weak, which limits the pull they are able to propagate [Bellahsen et al., 2005; Schellart, 2004b; Wu et al., 2008], thus presenting the challenge of how to reconcile the low apparent strengths with the efficient slab pull propagation required by global models to match plate velocities. In fact, the validity of these models of effective viscosity is based on the assumption that the complex layered rheological structure of the lithosphere [Goetze and Evans, 1979; Kameyama et al., 1999; Karato and Wu, 1993; Kohlstedt et al., 1995; Regenauer-Lieb et al., 2006a, 2006b] consisting of a weaker (partially brittle) top, a strong core, and a low-viscosity base, can be reduced to a one-layer setup with an averaged viscosity. Numerous theoretical studies of the behavior of a bending slab [Buckmaster et al., 1975; Buffett, 2006; Ribe, 2001] have shown that instead the balance between bending and stretching properties of a viscous plate vary as a function of the rheological layering. In particular, the resistance to bending decreases while the resistance to stretching increases if a stronger thin core is included [Capitanio et al., 2007].

[6] Here, we present a subduction model focused on the properties of the lithosphere. We implement two different sets of models: (1) a constant viscosity (isoviscous) plate and (2) a layered viscosity plate, where a high-viscosity core is embedded between two weaker layers. The two sets of models are formulated to have the same average effective viscosity. However, they have very different mechanical properties, as strength is distributed in the isoviscous model, but concentrated within the thin strong core in the layered model. Modeling subduction with these slabs, we find that the bending dissipates only a small portion of the total potential energy and scales with the moment applied by the slab, i.e., its buoyancy, while being largely independent of the viscosity and its distribution within the plate.

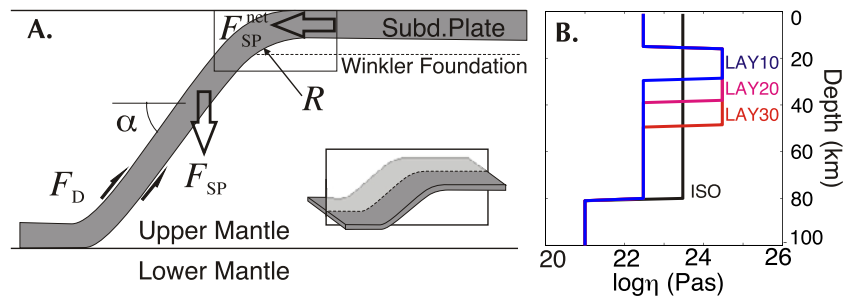


**Figure 1.** Sketch of the model setup. (a) Lithosphere is represented by a finite element model of  $2500 \text{ km} \times 80 \text{ km}$  ( $250 \times 20$  elements). Properties of the plate are constant along the strike of subduction. Mantle drag is for a plate with a finite  $1000 \text{ km}$  width. The model corresponds the center of plate (inset). Subduction is driven by slab pull ( $F_{SP}$ ) and resisted by mantle drag ( $F_D$ ), a Winkler Foundation at the plate base, and a density jump of  $10\%$  at the transition between upper and lower mantle, at  $660 \text{ km}$  depth. The radius of curvature  $R$  and net slab pull  $F_{SP}^{\text{net}}$  are measured in the bending area (rectangle)  $500 \text{ km}$  wide by  $250 \text{ km}$  deep. Dip  $\alpha$  is measured as the tangent of the slab at slab's middepth ( $330 \text{ km}$ ). (b) Distribution of viscosity in the different lithosphere models: constant throughout the plate ( $0\text{--}80 \text{ km}$ ) in the isoviscous (ISO) models and layered in models with a strong core extending  $10 \text{ km}$  (LAY10),  $20 \text{ km}$  (LAY20), and  $30 \text{ km}$  (LAY30) below the upper  $20 \text{ km}$  thick layer.

[7] We propose a formulation for the bending dissipation after *Buffett* [2006] and *Conrad and Hager* [1999] that incorporates our model result that bending radius increases with lithospheric viscosity such that bending dissipation does not depend on plate strength. Our formulation allows us to assess the relative bending dissipation in Earth's subduction zones, using parameters from recent global compilations [*Lallemand et al.*, 2005; *Wu et al.*, 2008]. We find that relative bending dissipation  $\Phi_B/\Phi_{\text{TOT}} < 20\%$ . The low bending dissipation and Earth-like strength layering, with a strong plate core, allow for high stress propagation to the surface plate, with a net slab pull  $F_{SP}^{\text{net}} = 1$  to  $6 \times 10^{12} \text{ N m}^{-1}$ , depending on slab buoyancy.

## 2. Model Setup

[8] The numerical set up used in this work is based on the method of *Capitanio et al.* [2007] and *Morra and Regenauer-Lieb* [2006a]. The finite element model ( $20 \times 250$  elements) of the subducting plate is a solid linearly viscoelastic body,  $80 \text{ km}$  thick,  $2500 \text{ km}$  long and  $1000 \text{ km}$  wide, without any along strike variations in properties or plate kinematics (Figure 1a and Table 1). The response of the fluid mantle is implemented as a dissipative drag force, proportional to the local velocity at the plate's surface, and (nondissipative) isostatic restoring force (Winkler foundation), allowing a free evolution of the plate surface. The local drag coefficients are calculated from the analytical 3-D Stokes drag for a  $1000 \text{ km}$  wide square plate sinking into an unbounded Newtonian fluid after *Capitanio et al.* [2007]. This is a good

representation of the interaction of the slab with a passive mantle [*Morra and Regenauer-Lieb*, 2006a]. The mechanical energy conservation equations are solved using the Arbitrary Lagrangian-Eulerian FE package ABAQUS [*Hibbit, Karlsson, and Soerenson Inc.*, 1999].

[9] In our models we vary lithospheric buoyancy from that appropriate for a young plate to that for an old oceanic lithosphere with an eclogitic crust [*Cloos*, 1993], by keeping the plate thickness  $H$  constant and varying  $\Delta\rho$ . We initiate subduction by pushing the tip of the slab down to  $150 \text{ km}$ , which is enough to induce self-sustained subduction. During their evolution, the slab models are confined to the upper mantle by a  $10\%$  increase in density at a depth of  $660 \text{ km}$ . (Models with a viscosity increase at  $660$  behave similarly). We do not focus on the evolution of the subduction, but measure curvature, stress and strain rates when  $60\%$  of the whole plate is subducted, i.e., when steady state subduction occurs.

[10] For the main results presented, the effective viscosity of the model plates is  $\eta^{\text{eff}}$  is around  $3 \times 10^{23} \text{ Pa s}$ , i.e., 300 times the viscosity of the mantle ( $\eta_L/\eta_{\text{UM}} = 300$ ,  $\eta_{\text{UM}} = 10^{21} \text{ Pa s}$ ), compatible with mineral physics and geoid constraints [*Karato and Wu*, 1993; *Mitrovica*, 1996]. However, we also ran several of the models with  $\eta_L/\eta_{\text{UM}}$  around 3000 for checking the viscosity sensitivity of the results. We test two rheological end-member models: an isoviscous lithosphere, where the plate viscosity is constant, and a lithosphere whose strength is concentrated in a thin strong core [*Morra and Regenauer-Lieb*, 2006b; *Regenauer-Lieb et al.*,

**Table 1.** Basic Model Parameters and Symbols

Parameter	Symbol	Value
<b>Lithosphere</b>		
Thickness	$H$	80 km
Mechanical thickness	$h$	
Core (Lay10)	$h_C$	10 km
Core (Lay20)	$h_C$	20 km
Core (Lay30)	$h_C$	30 km
Density	$\Delta\rho$	30.1, 49.65, 69.2, 88.75 kg m <sup>-3</sup>
Viscosity	$\eta_L$	$3 \times 10^{23}$ Pa s
Average effective	$\langle\eta^{eff}\rangle$	$\eta_L$
Isoviscous (Iso)		$\eta_L$
Core (Lay)	$\eta_C$	$3 \times 10^{24}$ Pa s
Outer lay. (Lay)		$3 \times 10^{22}$ Pa s
Resistance to bending	$Br$	
Iso	$Br$	1
Lay10	$Br$	0.02
Lay20	$Br$	0.15
Lay30	$Br$	0.5
Resistance to stretching	$Sr$	
Iso	$Sr$	1
Lay10	$Sr$	1.25
Lay20	$Sr$	2.50
Lay30	$Sr$	3.75
Width		1000 km
Initial length		2500 km
Slab length	$L$	
Curvature	$K$	
Curvature radius	$R$	$K^{-1}$
Young's mod.	$E$	$2 \times 10^{11}$ Pa
Poisson ratio	$\nu$	0.3
Gravity	$g$	$9.81$ m s <sup>-2</sup>
<b>Mantle</b>		
Thickness	$h_{UM}$	660 km
Density	$\rho_{UM}$	$3300$ kg m <sup>-3</sup>
Viscosity	$\eta_{UM}$	$10^{21}$ Pa s
Lower mantle transition	$\Delta\rho/\rho_{UM}$	10%

2006a, 2006b] (Figure 1b). We will only consider here the implications that such viscosity distributions have for slab bending and slab-plate coupling. We thus simplify the plate's viscosity distribution to its essence by embedding a strong viscoelastic core of  $\eta_C = 3 \times 10^{24}$  Pa s between two weaker viscoelastic layers of  $3 \times 10^{22}$  Pa s, and modeling a variable core thickness,  $h_C = 10, 20$  and  $30$  km, a range that might be expected for different age-dependent oceanic lithosphere geotherms. Although true plate rheological structure is complex and layered, with different deformation mechanisms as a function of pressure, temperature and stress, the simple layered rheology we use captures the essential characteristic that dissipation

in the top (partially brittle) and basal (low viscosity) layers is 2 or more orders of magnitude lower than that in the plate's interior [Regenauer-Lieb et al., 2006b].

[11] We measure the effective viscosity in our models as the Newtonian equivalent averaged over the volume  $\eta^{eff} = \int_V \sigma_{II}/2\dot{\epsilon}_{II} dV/V$  [Conrad and Hager, 1999], where the stress and strain rate invariants are not imposed, nor are they limited by plasticity. They are all within  $3 \pm 1 \times 10^{23}$  Pa s (or  $3 \pm 1 \times 10^{24}$  Pa s for the higher-viscosity cases). In our models we do not explicitly include the plastic behavior in any of the layers. Exceeding the bending stress might imply a nonlinear plastic failure at the trench hinge, a process still not fully understood. Instead, we will discuss the possibility that the lithosphere cannot sustain stresses larger than the yield limit [e.g., Turcotte et al., 1978; Turcotte and Schubert, 1982] of  $\sigma_Y = 500$  MPa [Goetze and Evans, 1979; Kohlstedt et al., 1995], and no greater stress can be achieved in the bending.

### 3. Mechanical Properties of Lithospheric Models

[12] Plate margins undergo two deformation regimes at the trench: tensile and bending [Ribe, 2001]. The resistance of plates to these regimes is described by two different mechanical properties: the tensile stiffness and the flexural stiffness. These are general mechanical properties of the material, and we will refer to these properties in our models as the resistance to stretching,  $Sr$ , and the resistance to bending,  $Br$ , respectively. The resistance to bending of a viscous plate is  $Br = \eta h^3/3$  [Ribe, 2001; Turcotte and Schubert, 1982] and the resistance to stretching is  $Sr = 2\eta h$  [Ribe, 2001]. These directly control the plate bending and the stress propagation through the plates, respectively. Therefore, the way the plate bends at the trench, and the amount of slab pull transmitted to the surface, scale differently with plate thickness. We will address these two aspects separately.

[13] The mechanical properties  $Br$  and  $Sr$  are related to the internal distribution of viscosity in the lithosphere and not just a function of the effective viscosity. They depend on the mechanical thickness and the viscosity of the strong portion of the slab. These are the whole thickness  $H$  and viscosity  $\eta_L$  in the case of the isoviscous plate. For a layered plate of strongly variable viscosity, the mechanical strength is dominated by the stiffest

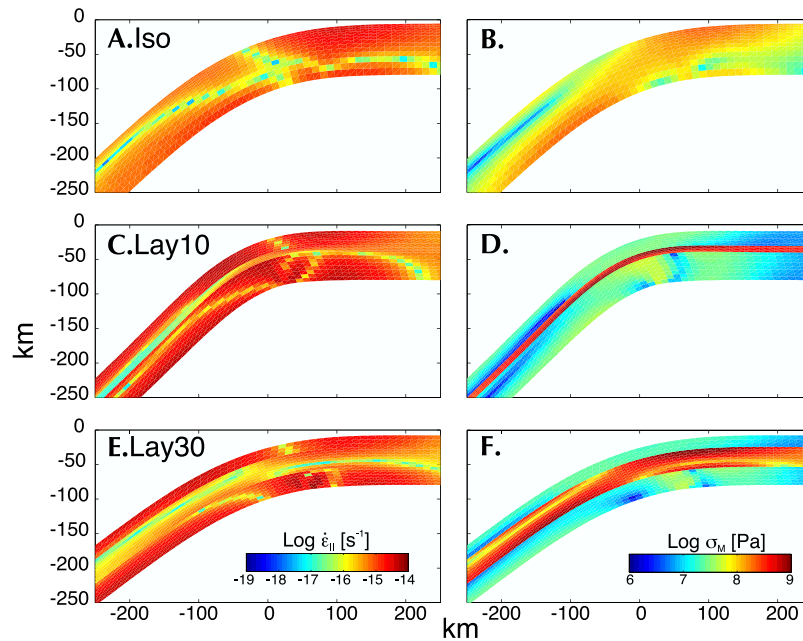


**Figure 2.** Distribution of strain rates and stresses in plate models with a density contrast  $\Delta\rho = 88 \text{ kg m}^{-3}$ . (a and b) Isoviscous model (ISO), (c and d) layered model with 10 km thick core (LAY10), and (e and f) layered model with 30 km thick core (LAY30).

part, the core, hence the core's properties control  $Br$  and  $Sr$ . The values used here are  $H = 80 \text{ km}$  and  $h_C = 10, 20$  and  $30 \text{ km}$ , and  $\eta_L = 3 \times 10^{23} \text{ Pa s}$  and  $\eta_C = 3 \times 10^{24} \text{ Pa s}$ , corresponding to the thickness and viscosity of isoviscous plate and of the core, respectively. Using the isoviscous plate as reference,  $Br$  of the layered plates is  $\sim 0.02, 0.15$  and  $0.5$  times the isoviscous plates, while  $Sr$  is  $\sim 1.25, 2.5, 3.75$  times higher than isoviscous plates (Table 1). As a result of the dependence on the cube of the thickness, concentrating the strength in the core decreases the resistance to bending dramatically, from one half to almost hundred times, while increasing up to four times the resistance to stretching. This illustrates that the lithosphere-mantle viscosity contrast or average effective viscosity are not an appropriate measure of plate bending properties.

[14] Thinning of the plates while bending, i.e., varying thickness  $\Delta h$ , plays an important role in modifying the mechanical properties of the plate [Capitanio *et al.*, 2007]. The stretching resistance reduces as  $\Delta h$ , while the bending resistance  $Br$  reduces as  $h^2 \Delta h$ . Therefore, a small amount of thinning can significantly change the bending stresses as well as reducing the resistance to subsequent deformation, possibly inducing a fast strength reduction. Furthermore, the bending cur-

vature radius and the thinning control the stress achieved in the bending plate, as the stresses are proportional to the bending moment  $M = Br\dot{K}$  [Ribe, 2001], where the rate of the curvature  $\dot{K} = \partial K / \partial t$ , and curvature  $K$  is defined in the next section.

## 4. Results

### 4.1. Plate Bending

[15] In Figures 2 and 3 we show a cross section of the plate in the bending area, centered on the position of the maximum (negative) curvature in the bending,  $x_0 = 0$ . The distributions of stress and strain are strongly controlled by the internal layering of viscosity. Stress and strain rates are distributed in the isoviscous model, whereas in the layered models larger stress is achieved in the stiff core (Figures 2b and 2e). Low stretching in the core prevents the whole plate from stretching, limiting the strain rates everywhere in the plate (Figures 2a and 2d). All the models attain very similar subduction and roll back velocities [Capitanio *et al.*, 2007] as well as dips, for the same buoyancy (Figures 3a and 5b). Velocities increase and dips decrease with increasing buoyancy, where minor differences in dip are due to the plate's mechanical properties ( $\pm 3-5^\circ$ ).

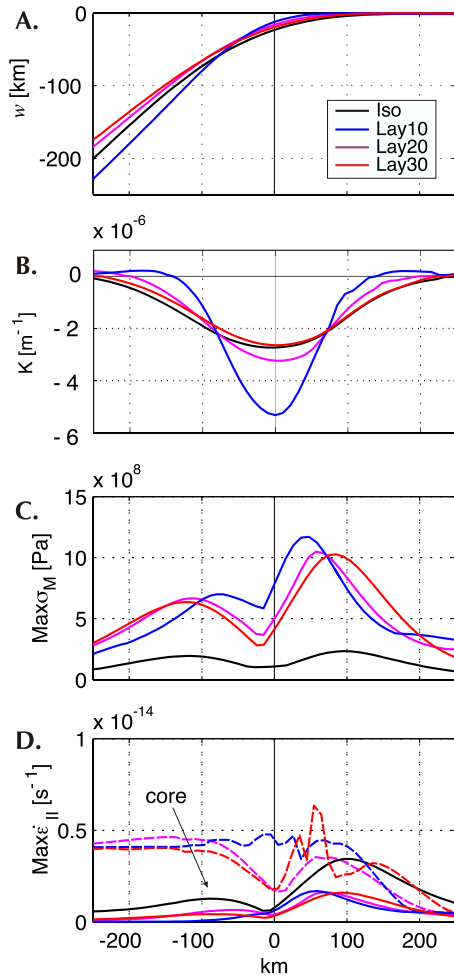


**Figure 3.** Profiles along the plate in the bending area for different models of same buoyancy ( $\Delta\rho = 88 \text{ kg m}^{-3}$ ), centered around the maximum curvature point  $x_0 = 0$ : (a) Deflection  $w$  in bending. (b) Curvature  $K$  ( $R^{-1}$ ). (c) Maximum Mises stress. (d) Maximum in-plane strain rates in the plate (ISO) or cores (LAY) (solid lines). Maximum strain rates in the core of layered models are lower than in the outer layers (dashed).

[16] The curvature  $K$  and bending radius  $R$  (Figure 3b) are defined as:

$$K = \frac{1}{R} = \frac{w''}{\sqrt{(1 + w'^2)^3}}, \quad (1)$$

where  $w$  is the deflection (Figure 3a),  $w' = \partial w / \partial x$  and  $w'' = \partial^2 w / \partial x^2$ . The curvature, and hence the radius, is continuously varying and almost symmetrical around its maximum curvature point,  $x_0$  (Figure 3b). The area of the slab where the curvature is nonzero defines the bending zone. This extends from the point of maximum (negative) curvature to a distance of 250 km in both directions, extending to depth of  $\sim 250$  km (Figures 2a and 3a).

[17] Larger Mises stresses are achieved in the layered plates (Figure 3c), up to 5 times those of the isoviscous plate, and are always localized in the core. In layered plates, strain is larger in the outer layers (Figures 2 and 3d, dashed lines) and very low in the core (Figures 2 and 3d), where strain rates are a factor of 0.5 to 0.3 less than in the isoviscous case and outer weaker layers, respectively. The stress values at the end of the bend area (250 km) give an estimate of the propagation to the plate at surface (Figure 3c). Stresses up to 200 to 300 MPa can be transmitted to the surface plates.

[18] Figure 4 illustrates that in general isoviscous plates have higher maximum strain rates,  $0.25\text{--}6 \times 10^{-15} \text{ s}^{-1}$ , and lower maximum stresses, 40–120 MPa, than layered plates, where the strain rates in the core are as low as  $0.3\text{--}1 \times 10^{-15} \text{ s}^{-1}$  and stresses as high as 250–700 MPa. Possibly, plates of buoyancy larger than  $80 \text{ kg m}^{-3}$  would yield in nature (Figures 2 and 3 and the gray area in Figure 4), since these reach average Mises stresses above the laboratory yield limit  $\sigma_Y = 500$  MPa.

[19] Our model includes elasticity as a component of Maxwell viscoelasticity. This implies that elasticity plays a role only for strain rates larger than  $\tau_M^{-1}$ , where  $\tau_M$  is the Maxwell time [Funiello *et al.*, 2003]. For the parameters used here  $\tau_M^{-1} = 10^{-12}\text{--}10^{-13} \text{ s}^{-1}$ . Because the strain rates in our models are mostly much lower than such a threshold, the stress distribution in the plate differs from

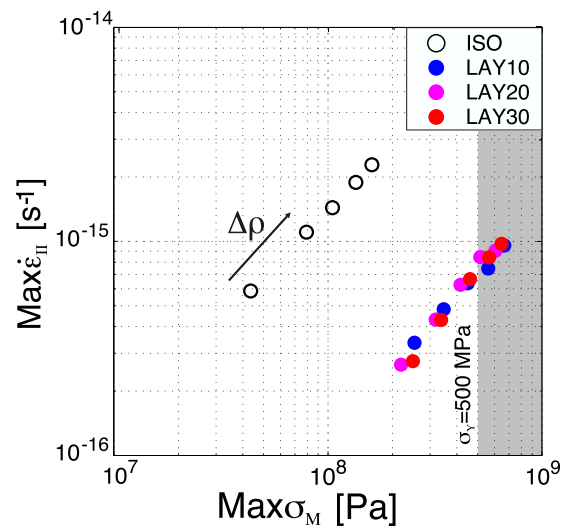


**Figure 4.** Maximum strain rates versus maximum Mises stresses. Increasing buoyancy ( $\Delta\rho$ ) increases stress and strain rates. Isoviscous models attain larger strain rates and lower stresses than the layered models. Gray indicates the area where Mises stress exceeds a potential yield stress of 500 MPa.

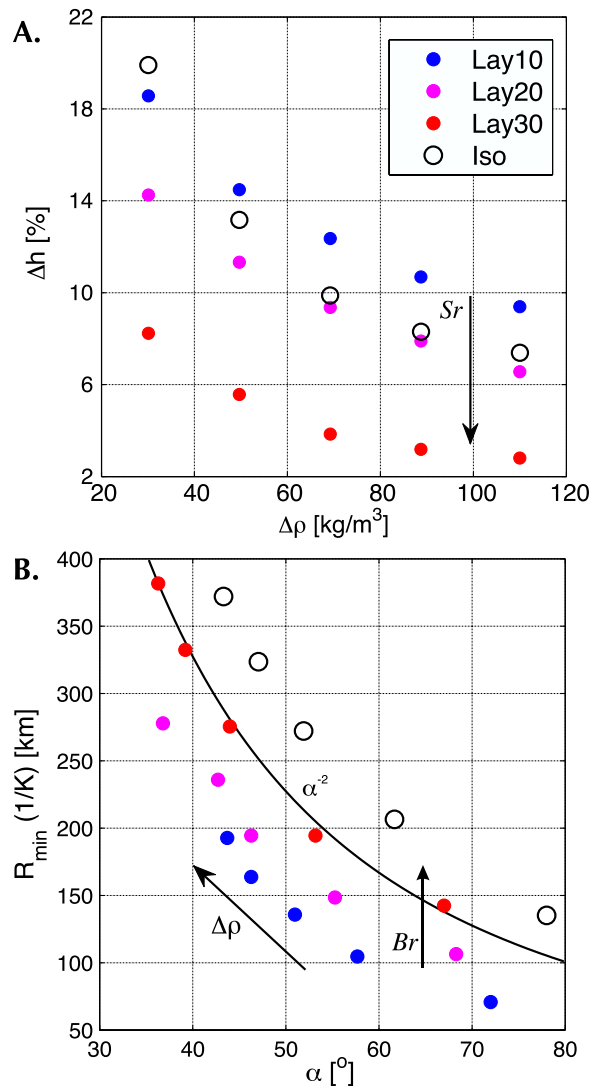


**Figure 5.** (a) Thinning percentage of the plates versus buoyancy. The thinning is measured in the whole plate for the isoviscous models and in the core in the layered models. Larger thinning is achieved in lower-buoyancy plates. The resistance to stretching ( $Sr$ ) exerts the main control on the thinning of plates. (b) Minimum curvature radius versus the dip. Radii and dips are anticorrelated, where less buoyant plate models achieve the steepest dips and smallest radii.  $R_{\min}$ , measured in the point of maximum curvature, varies strongly according the thickness of the core, whereas variations in dip with rheology are minor.

that of the elastic bending. In fact, in purely elastic models, the stress is expected to be concentrated around the point of maximum curvature and to be symmetrical laterally and vertically, but with opposite sign on each side of  $x_0 = 0$  [Turcotte and Schubert, 1982]. Although the curvature of the viscoelastic plate is very similar, the largest stress

and strain rates are not achieved in the point of maximum curvature. Rather, during the bending and unbending, large stresses occur at the top and bottom of the plate (Figures 2a and 2b). The largest bending deformation occurs on the first flank of the bending. Here the stresses and strain rates are  $\sim 4$  times larger than those in the unbending flank, in all the models (Figures 3c and 3d). Because of the effect of thinning on the mechanical properties, the weakening is achieved almost completely on the bending flank toward the trench, where the thinning drops the resistance to further bending and stretching in the unbending flank. This effect will be enhanced in the real Earth where increasing temperatures with depth will induce a weakening of the plate, thus further reducing the already minor dissipation in the unbending region.

[20] The maximum Mises stresses and strain rates measured are almost the same for the different layered models with the same plate buoyancy (Figures 3c, 3d, and 4), indicating they have a similar effective “strength.” Even though effective viscosity estimates of the isoviscous and layered models are similar, the effective “strength” in bending for the isoviscous cases is lower than that for the layered cases, resulting in lower stresses and higher strain rates. The trends in Figure 5 indicate that plate thinning, together with adjustments in the radius of curvature and final dip limit the excess differential stresses in the bending layers, making the main driving force, i.e., slab pull, the dominant control on maximum stress, maximum strain rate and, as we will discuss below, bending dissipation.

[21] The total thinning  $\Delta h$  achieved in the bending is different for models with different initial  $h$  and  $Sr$ , ranging from few percent for high  $Sr$  plates (Lay30), to a maximum of 20% in the plates with the lowest  $Sr$  (Iso) (Figure 5a). This suggests that thickness accommodation assists in limiting stress and strain rates in the bend, by partially adjusting the different initial mechanical properties of each plate toward a similar effective resistance. Larger thinning is associated with lower buoyancy, because at the lowest rates there is more time to achieve bending-induced stretching [Ribe, 2001]. Minimum curvature radii  $R_{\min}$ , measured in  $x_0$ , range between 50 and 400 km (Figure 5b), increasing with the buoyancy of the plate by a factor  $\sim 2.6$ , for the range tested. The bending radius scales with the resistance to bending: the Iso and Lay30 plates, with higher  $Br$ , have 2 to 3 times larger radii than the thinner core plates. The min-

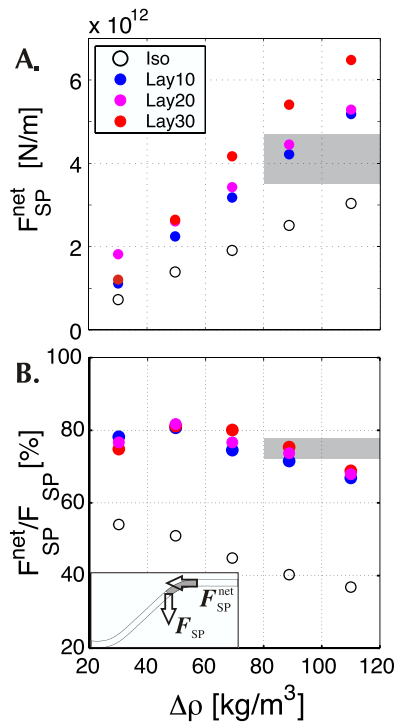


**Figure 6.** (a)  $F_{SP}^{\text{net}}$  versus plate buoyancy.  $F_{SP}^{\text{net}}$  is measured at 250 km from the maximum curvature point (see inset in Figure 6b). Net slab pull increases with plate buoyancy. Layered models all attain similar pull, with minor variations due to the rheology, which is up to twice isoviscous plate slab pull. Gray indicates the area where Mises stresses are larger than a potential yield stress of 500 MPa (Figure 5). (b) Net propagation of pull forces through the bending area. The slab pull  $F_{SP}$  is measured at deeper end of the bend (gray area in the inset). Percentage of the net slab pull in the layered models (66–82%) is larger than in the isoviscous ones (38–56%) and increases with decreasing buoyancy. Gray indicates the area where Mises stress exceeds 500 MPa (Figure 5), possibly limiting force propagation to a minimum of 75%.

imum curvature radius  $R_{\text{min}}$  is as low as 70 km in lowest  $Br$  plate (Lay10) and up to 400 km in Lay30 and Iso models, which have similar (normalized)  $Br$ , of 1 and 0.5, respectively (Figure 5b). The radius of curvature decreases with decreasing buoyancy, i.e., with increasing deformation time.

[22] A general result is that, independently of the rheology employed and the type of layering tested, all the models show an anticorrelated trend between radii and dips (Figure 5b). The trend is toward larger radius and shallower dip for increasing slab pull, i.e., buoyancy, and is well fit with a trend of  $R$  proportional to  $\alpha^{-2}$  (Figure 5b). Over the range of  $Br$  considered, radius scales by up to a factor 3 with increasing  $Br$ , while dip decreases by

less than  $8^\circ$ . Slab dip angle is mainly controlled by the bending moment due to the slab's buoyancy, and not strongly affected by core thickness, but bending radius adjusts to limit excess stress and bending dissipation.

## 4.2. Net Slab Pull Force and Force Propagation

[23] The force transmitted to the unsubducted part of the plate is referred to as the net slab pull  $F_{SP}^{\text{net}}$ , that is the force generated by the slab pull, after accounting for its partial balance by resistive mantle forces (viscous drag), and propagated through the bending to the plate. We extract  $F_{SP}^{\text{net}}$  from our models as in the works by Buffett [2006] and Ribe [2001]:

$$F_{SP}^{\text{net}} = N = \int_{-H/2}^{H/2} \sigma_{ss} dz \quad (2)$$

measured at 250 km from  $x_0$ , out of the bending zone, in the unsubducted plate, where  $s$  is the in-plane direction in the slab.

[24] The net slab pull force  $F_{SP}^{\text{net}}$  varies between 0.7 and  $6.5 \times 10^{12} \text{ N m}^{-1}$  (Figure 6a) and increases linearly with increasing plate density in all models. The  $F_{SP}^{\text{net}}$  in the layered lithospheres ranges between 1 and  $6.5 \times 10^{12} \text{ N m}^{-1}$ , for the minimum and maximum densities tested, respectively, i.e., increasing 5–6 times, whereas net slab pull in the isoviscous models increases  $\sim 4$  times from 0.7 to  $3.1 \times 10^{12} \text{ N m}^{-1}$ . The net pull force in the layered plates is twice that of the isoviscous models, and increases with increasing resistance to stretching  $Sr$ . As observed earlier, plastic yielding of plates might limit force propagation, in the same way it limits differential bending stresses. In this case,  $F_{SP}^{\text{net}}$  will be limited in plates with a density larger than  $\sim 80 \text{ kg m}^{-3}$  (Figure 6a, gray area). Thus, possibly no force larger than  $3.5\text{--}4.5 \times 10^{12} \text{ N m}^{-1}$  can be transmitted.

[25] The net slab pull  $F_{SP}^{\text{net}}$  is then compared to the total negative buoyancy of the slab, to estimate how much of the pull propagates through the bend (Figure 6, inset). The layered models propagate larger amounts of slab pull than the isoviscous plates.  $F_{SP}^{\text{net}}$  is estimated to be 38–56% for the isoviscous models and 68–82% for the layered ones, but not less than  $\sim 75\%$  if considering the limiting effect of plasticity. Net slab pull percent decreases with increasing buoyancy. The pull propagation in layered plates is different from the isoviscous plate, but it is almost the same for the

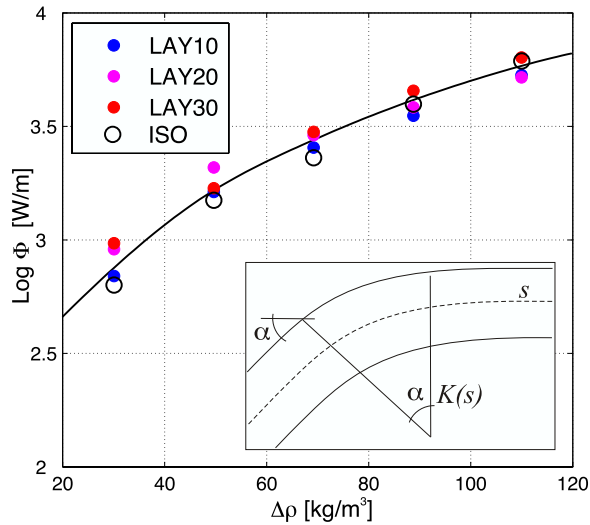


**Figure 7.** Model dissipation in the bending  $\Phi_B$  compared to predicted dissipation using equation (8), where  $R$  scales with effective viscosity. All the models, irrespective of their rheology, attain similar bending dissipation for increasing buoyancy, with variations less than 20% around the analytic trend. The inset shows a sketch of the bending area with parameters used in the formulation of section 4.3.

three core thicknesses modeled. Again this reflects that effectively the layered plates are stronger than the isoviscous plates, and that there is little difference in effective strength between the layered plates with different core thicknesses due to thinning and curvature adjustments (Figure 5). Hence, a realistic thin core has the power of controlling the net slab pull force propagated through the plates (Figure 6).

### 4.3. Dissipation

[26] Characterizing patterns of energy dissipation and its partitioning between intraslab deformation and slab-mantle interaction provides an understanding of subduction dynamics and allows for some predictions on the geometrical and kinematic characteristics of subduction zones on Earth. We measure lithospheric dissipation as in the work by *Capitanio et al.* [2007], after *Ranalli* [1987]:

$$\Phi = \int_V \sigma_{ij} \dot{\epsilon}_{ij} dV \quad (3)$$

where  $\sigma_{ij}$ ,  $\dot{\epsilon}_{ij}$  and  $V$  are the stress tensor, the strain rate tensor and lithospheric volume, respectively. To obtain bending dissipation  $\Phi_B$ , we integrate over the bending zone, i.e., over plate thickness and over slab length between  $x = -250$  km and  $+250$  km.

[27] Our dynamically free subduction models show that bending dissipation is mainly controlled by plate buoyancy (Figure 7) and is, surprisingly, almost independent of the resistance to bending of the lithosphere. Bending dissipation ranges from 600 to 6000 W/m. There is a small effect of rheology on dissipation for models under the pull of low-buoyancy plates, because plate stretching is enhanced by their low subduction rates. These trends are in agreement with what was observed in the average stresses and strain rates (Figure 4), where maximum stresses and strain rates displayed limited control of rheology.

[28] Bending is an energetically expensive process, and bending dissipation increases rapidly with decreasing radius of curvature or increasing lithospheric viscosity (equation (5)) [*Conrad and Hager*, 1999]. To achieve subduction with the maximum efficiency (low internal dissipation for fast motion), fully dynamic plates adjust their curvature such that dissipation in the trench is relatively small, thereby minimizing the dependence of dissipation, and maximum stress and strain rates, on lithospheric viscosity or plate viscosity structure.

[29] We show here how this model outcome modifies the analytical treatment proposed by *Buffett* [2006] and *Conrad and Hager* [1999] and its implications for plate dynamics at the trench. Following *Buffett* [2006], dissipation in the bend is a function of plate geometry and subduction velocity. The contribution of plate geometry can be summarized in an integral as a function of the curvature along the plate's length:

$$\Phi_B = \frac{1}{3} \eta_L u_0^2 H(s)^3 \int_0^L \left( \frac{dK(s)}{ds} \right)^2 ds \quad (4)$$

where  $\eta_L$  is a measure of effective lithospheric viscosity,  $u_0$  is plate velocity,  $H(s)$  is lithospheric thickness, and  $K(s)$  is the integrated curvature over the slab's length  $L$ . The integral in (4) can be approximated as:

$$\int_0^L \left( \frac{dK(s)}{ds} \right)^2 ds = \int_0^{\alpha R} \left( \frac{dK(s)}{ds} \right)^2 ds = \frac{\alpha c_1}{R_{\min}^3} \quad (5)$$

where  $c_1$  is a constant that depends on the local bell shape of the curvature along the along-slab coordinate  $s$ , and  $\alpha$  is the plate dip (Figure 7, inset).

[30] Our treatment differs from *Buffett* [2006] and *Conrad and Hager* [1999] as we propose a model where the radius of curvature varies with plate

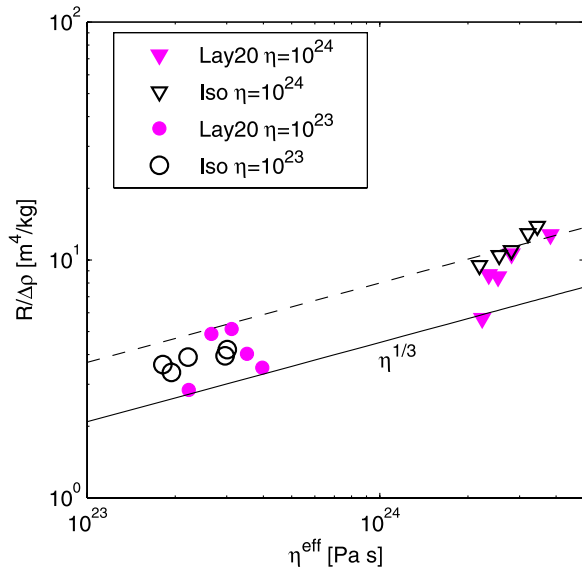


**Figure 8.** Curvature Radii  $R_{\min}$  normalized to the buoyancy  $\Delta\rho$  versus the effective viscosity  $\eta^{\text{eff}}$  measured in the models. Additional models Iso and Lay20 of a larger viscosity ( $3 \times 10^{24}$  Pa s) are also plotted. The increase of curvature radii is small and can be approximately fitted with a trend  $\sim \sqrt[3]{\eta^{\text{eff}}}$ .

strength, rather than choosing a constant value. On the basis of our numerical models' outcome that lithospheric dissipation, given plate thickness, does not vary with effective lithospheric viscosity (or actually with any of our measures of effective plate strength), we find an expression for the radius of curvature as a function of the mechanical properties of the subducting plate.

[31] All the models display minimal thickness variations, therefore we can assume  $H(s) = H$  and rewrite (5) as:

$$\Phi_B = \frac{1}{3} \eta_L u_0^2 \left( \frac{H}{R} \right)^3 \alpha c_1. \quad (6)$$

In order to eliminate the dependency of bending dissipation on lithospheric viscosity,  $\alpha/R^3$  needs to be proportional to  $\eta_L$ . To test this scaling, we have expanded the range of model viscosities, and run two additional sets of models (Iso and Lay20), at a higher viscosity ( $10^{24}$  Pa s). In Figure 8, we plot the radii normalized to the density versus the effective viscosity, defined in section 2. Radii of ten times stiffer plates increase only slightly, and can be fit by a trend proportional to  $\sim \sqrt[3]{\eta^{\text{eff}}}$ . Similar tests for dip (not shown) illustrate that it varies only as approximately  $(\eta^{\text{eff}})^{-1/6}$ . As shown,  $R$  varies much more strongly with plate viscosity

than  $\alpha$  does. Hence as a first approximation, we neglect the viscosity dependence of dip, and we propose the following scaling for the radius of curvature,  $R = c_2 \sqrt[3]{\eta_L}$ , where  $c_2$  is a scaling parameter.

[32] The  $R$ - $\eta_L$  scaling is consistent with results from the laboratory models of *Di Giuseppe et al.* [2008] and *Schellart* [2008], where for a 10 times viscosity increase, the bending radius increases from 100 to 200 km to 300 km (the recumbent large fold mode III of *Bellahsen et al.* [2005]), thus suggesting a similar  $\sim \sqrt[3]{\eta}$  scaling.

[33] Bending dissipation then simplifies to:

$$\Phi_B = (1/3) u_0^2 H^3 \alpha c_1 c_2 \quad (7)$$

Subduction velocity can be estimated with the Stokes-like formulation  $u_0 \approx v_{\text{Stokes}} \approx \Delta\rho g H L_0 / (24\sqrt{2} \eta_{\text{UM}}) = c_3 \Delta\rho g H L_0 / \eta_{\text{UM}}$  [*Capitanio et al.*, 2007], where  $c_3 = 1/(24\sqrt{2})$ , so (7) becomes:

$$\Phi_B = \left( \frac{\Delta\rho g H L_0}{\eta_{\text{UM}}} \right)^2 C \alpha H^3 \quad (8)$$

where  $C = (1/3) c_1 c_2 c_3^2$ . This formulation now reflects that bending dissipation is decoupled from the plate's rheological response and depends mainly on subduction rate. Note that dip  $\alpha$  varies inversely with density (Figure 5b), thus modulating the overall dependence of  $\Phi_B$  on density.

[34] A value for  $C$  can be estimated from a fit to the model values for  $\Phi_B$  (Figure 7),  $\alpha$  (Figure 5),  $H$  ( $= H_L$  or  $h_c$ ), and  $L_0$  ( $= 1000$  km). This gives constant  $C = 2.32 \times 10^3$ . Model deviations from the trend of equation (8) are  $\pm 10\%$ , increasing to  $\pm 20\%$  in the low-buoyancy plates. The same dissipation formulation and value of  $C$  also match the models with higher viscosity  $3 \times 10^{24}$  Pa s,  $\eta_L/\eta_{\text{UM}} = 3000$  (Figure 9), further corroborating the independence of dissipation from viscosity. The stronger-plate models slightly increase the variation around the trend, up to  $\pm 25\%$ , reflecting additional second-order complexities not captured by equation (8). But overall equation (8) provides a good description of the model results, and the scaling of  $R \propto \sqrt[3]{\eta_L}$  fits the model trends, while an expression with a constant  $R$  and  $\alpha$  clearly does not.

[35] Bending dissipation estimates for a formulation with constant radius and dip, using the values of viscosity and thickness proposed previously and our velocity range, increase strongly with viscosity, which is contrary to what is found in our models,

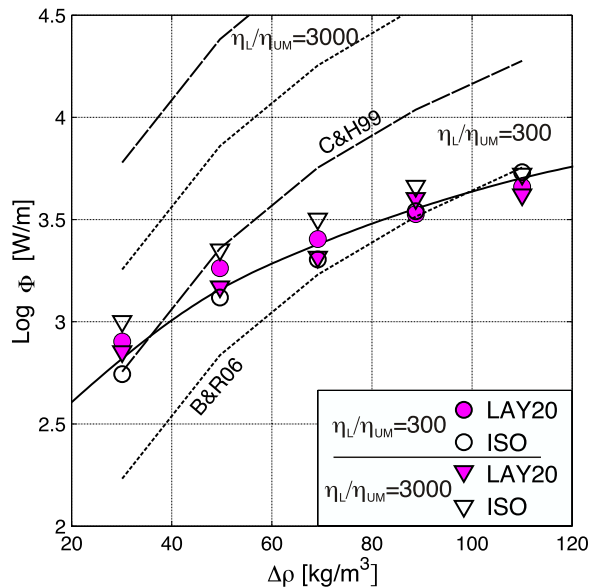


**Figure 9.** Bending dissipation for models of different viscosity contrast between plate and mantle. White indicates isoviscous models, and purple indicates LAY20 models. Circles are for a viscosity contrast of  $\eta_L/\eta_{UM} = 300$ , and triangles are for  $\eta_L/\eta_{UM} = 3000$ . Model fit from equation (8) (same as in Figure 7). *Conrad and Hager* [1999] (C&H99) and *Buffett and Rowley* [2006] (B&R06) bending dissipation analytical formulations are plotted for the values proposed by the authors ( $h_L = 100$  and  $R = 400$  km for C&H99 and  $h_L = 50$  km and  $R = 200$  km for B&R06), the velocities of our models, and a viscosity contrast of 300 and 3000.

and they increase more strongly with density than what is observed in the models (Figure 9).

## 5. Discussion

### 5.1. Estimating Dissipation in Natural Subduction Zones

[36] We have shown that plate mechanical properties control essentially the plate's bending radius, however they do not affect bending dissipation, which is rather controlled by the slab buoyancy and mantle viscosity. In our models as radius increases, the dip angle shallows. This behavior has also been observed in laboratory models of free subduction [Bellahsen *et al.*, 2005; Schellart, 2004a], suggesting that this might be a natural response of plates in a subduction system.

[37] The same relationship is found for subduction zones on the Earth, as revealed by the radii and dips of recent compilations [Lallemand *et al.*, 2005; Wu *et al.*, 2008]. For upper mantle confined subduction zones (Figure 10a, filled circles),  $R$  and

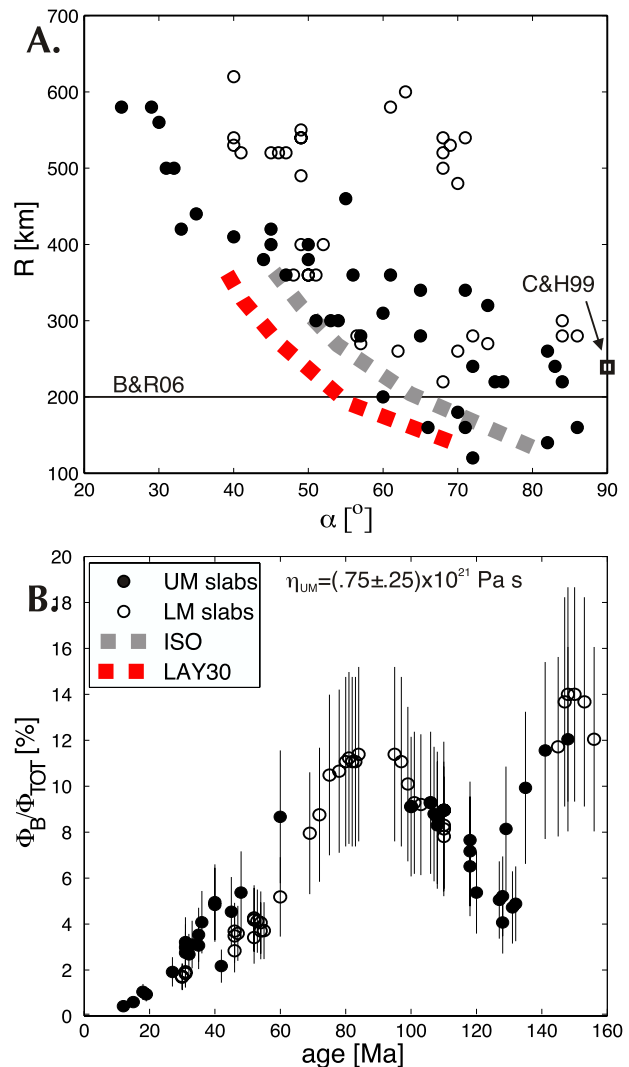


**Figure 10.** (a) Radius of curvature versus dip of observed subduction zones in the world from a compilation by *Lallemand et al.* [2005] and *Wu et al.* [2008]. Slabs reaching and laying over the transition zone at 660 km depth are shown as filled circles; slabs penetrating deeper in the lower mantle are shown as open circles. Trends of our numerical models (Figure 5b) for ISO (gray dashed thick line) and LAY30 models (red dashed thick line) are plotted for comparison.  $R = 200$  km gray line labeled B&R06 shows the values used by *Buffett and Rowley* [2006], Grey square labeled C&H99 corresponds to the values used by *Conrad and Hager* [1999] with  $R = 240$  km and  $\alpha = 90^\circ$ . (b) Bending dissipation percentage as computed following the analytical formulation (10) versus age. Error bars for  $\eta_{UM} = 0.75 \pm 0.25 \times 10^{21}$  Pa s. For plate thickness, we use a half-space thermal cooling model with a cutoff to constant thickness in plates older than 80 Ma.



$\alpha$  vary as in our models. Data are more scattered in bending plates contiguous to slabs penetrating deeper in the lower mantle (open circles).

[38] Several data points with radii larger than our models', as well as shallower dips, are still in the trend defined by our models. A larger pull than what was considered in the models, or a stronger plate (like those with  $\eta_L/\eta_{UM} = 3000$ ) might explain these points. Additional force contributions from ridge push and trench suction slightly increase the net torque at the bending [Capitanio *et al.*, 2007], yielding larger values of  $\alpha$ , compatible with the direction most of the data points are shifted in relative to the models shown in Figure 10a. Plates contiguous to lower mantle slabs may be subject to other additional forces.

[39] We now apply the bending dissipation formulation from equation (8) to the natural subduction zone data. The total energy dissipated in the system, i.e., potential energy, is defined, following Buffett and Rowley [2006], Capitanio *et al.* [2007], and Conrad and Hager [1999], as:

$$\Phi_{TOT} = \Phi_{POT} = F_{SP} v_{sink} = \Delta \rho g H L v_{Stokes}. \quad (9)$$

Relative dissipation in the bending hence reduces to:

$$\Phi_B / \Phi_{TOT} = \frac{D \alpha H^3}{\eta_{UM}} \quad (10)$$

where  $D = C 24\sqrt{2}$ . Since plate thickness in nature varies with the thermal age of the plate, we can describe it as a function of age  $t$  at the trench as  $H = 2.32(\kappa t)^{1/2}$  [Turcotte and Schubert, 1982], where  $\kappa$  is the thermal diffusivity. Therefore, the relative bending dissipation is  $\Phi_B / \Phi_{TOT} \propto \alpha t^{3/2} / \eta_{UM}$ . We cut off plate thickening when the age is  $> 80$  Ma, to reconcile with the observations of ocean bathymetry and heat flux [Stein and Stein, 1992].

[40] Using the dips and age at trench of the compilations, we obtain a relative bending dissipation below 20% (Figure 10b). The main uncertainty in this estimate is due to the estimate of mantle viscosity used. Bars in Figure 10b cover a range of possible upper mantle viscosities of 0.5 to  $1 \times 10^{21}$  Pa s. Our estimates are slightly lower than the  $\sim 25\%$  found by Wu *et al.* [2008], who constrained dissipation with a global mantle flow model and observed variable values of  $R$ .

[41] The relative bending dissipation is a strong function of age, which can be understood if we

consider that younger plates are (1) relatively thin, and thus weak in the bending, and (2) less dense, i.e., exert lower slab pull than older plates. The trend in dissipation versus age breaks down in plates older than  $\sim 90$  Ma. This may be due to a variability in the change in the factors controlling plate thickness for these old plates, or possibly the bending can be affected by failure, so that the hinge experiences plastic dissipation which is not accounted for in our models. Plastic dissipation in the hinge might be higher than what we obtain from our models [Di Giuseppe *et al.*, 2008]. However, the mechanisms of the plastic hinge failure are not well constrained, and estimates are speculative. We have included in our estimates the effect of the larger thinning experienced by slower plates. This might be enhanced on Earth, where the temperature dependence of viscosity possibly increases the dissipation in the bend of very young plates.

[42] In subduction zones where the plate at the trench is younger than  $\sim 90$  Ma, we observe that dissipation in the bending is slightly higher in slabs penetrating into the lower mantle than those confined to the upper mantle. This suggests that large forces from the deeper mantle act on the bend, adding to upper mantle slab pull. This is in agreement with numerical global flow models [Becker and O'Connell, 2001; Conrad and Lithgow-Bertelloni, 2002] and observed plate motions [Goes *et al.*, 2008], which indicate that lower mantle flow enhanced by deep penetrating slabs provides a significant contribution to subduction driving forces. They possibly also increase the forcing on the trench bends.

## 5.2. Comparison With Previous Dissipation Estimates

[43] Several models have predicted plate motions by evaluating the bending dissipation [Buffett and Rowley, 2006; Conrad and Hager, 1999; Faccenna *et al.*, 2007; Wu *et al.*, 2008], assuming that the stiff plate resists bending at trench, opposing slab pull forces. These estimates were based on the analytical expression of bending dissipation in equation (6),  $\Phi_B = (2/3)(H/R)^3 \eta_L u_0^2$ , with the assumption that radius, dip, and thickness of the plate are constant, and dissipation depends on variable viscosity. With these assumptions, bending dissipation increases rapidly for increasing velocity, so that the larger the subduction velocity is toward the trench the lower the net slab pull becomes [Wu *et al.*, 2008], leaving it unclear which force drives the fast motions. This is at odds with our results and



other numerical and laboratory models [Bellahsen *et al.*, 2005; Capitanio *et al.*, 2007; Di Giuseppe *et al.*, 2008; Schellart, 2008] where subduction motions for viscosity contrast up to  $10^3$  are not hampered and dissipation partitioning does not essentially change. In their work, Wu *et al.* [2008] find that the match between their models and observed plate motions improves for decreasing viscosity contrast. This strongly suggests that the bending at subduction zones on Earth does not represent an impediment to slab pull drive.

[44] The estimates provided by our formulation support the idea that the resistance to bending is low [Stegman *et al.*, 2006; Wu *et al.*, 2008]. However, several models proposed larger values of bending dissipation. Becker *et al.* [1999] found very high bending dissipation. However, their study focuses on the initiation of subduction, which is dominated by the viscous thickening of the initial instability, and is likely characterized by a different energy partitioning than later stages of plate subduction. Several other models show that plastic failure during bending might strongly affect the dissipation, which may be as low as 18% [Stegman *et al.*, 2006], or range up to 30–50% [Di Giuseppe *et al.*, 2008]. However, plastic failure may affect only a few subduction zones [Turcotte *et al.*, 1978].

[45] Furthermore, previous estimates of bending dissipation rely on the magnitude of driving pull of upper mantle slabs only [Buffett, 2006; Conrad and Hager, 1999; Faccenna *et al.*, 2007; Wu *et al.*, 2008], whereas our dissipation estimates for subduction zones above lower mantle penetrating slabs suggest that the bending is possibly sensitive to additional forces other than just the upper mantle slab pull. This might be relevant during the evolution of the subduction system, when slabs penetrate in the lower mantle, as suggested by numerical models [Becker and O'Connell, 2001; Conrad and Lithgow-Bertelloni, 2002] and observations [Goes *et al.*, 2008].

### 5.3. Role of Slab Pull Propagation

[46] The solutions of bending behavior based on using constant radii, viscosities and plate-incoming velocity [e.g., Buffett, 2006; Buffett and Rowley, 2006; Wu *et al.*, 2008] imply in general higher energy dissipation at the trench compared to our models. Our estimates allow a larger propagation of slab pull, in agreement with the high pull transmission required to match plate motions

[Conrad and Lithgow-Bertelloni, 2002, 2004]. Our models show that the dissipation and the propagation of the pull force are two distinct aspects. While the dissipation is the result of the applied bending moment to the plate, i.e., the plates' buoyancy, and largely independent of the plates' inner properties, the propagation through the bend depends only on the continuity of a stress guide inside the plate [e.g., Elsasser, 1969], which is facilitated by the strong thin core. Although the plate's effective viscosity has a control on the subduction motions, defining plate advance and trench retreat partitioning [Bellahsen *et al.*, 2005; Capitanio *et al.*, 2007; Di Giuseppe *et al.*, 2008; Faccenna *et al.*, 2007; Funiciello *et al.*, 2003; Schellart, 2008], it does not appropriately describe the ability of plates to bend and propagate stress to plates at surface.

[47] For plates with a strong thin core, net slab pull  $F_{SP}^{net}$  propagated through the bend is as large as 70–80% of the total negative buoyancy. This is in agreement with global models that require 70–100% slab pull transmission [Conrad *et al.*, 2004]. Our net slab pull is close to laboratory estimates of  $\sim 4.1\text{--}6.1 \times 10^{12} \text{ N m}^{-1}$  [Schellart, 2004b] and inversion of trench bulges in various tectonic settings that has yielded slab pull of  $3\text{--}12 \times 10^{12} \text{ N m}^{-1}$  [Royden, 1993]. Large stresses (up to 200 to 300 MPa) are propagated through the bend to the plates at surface. Stress propagation is possibly limited by plastic yielding, and net slab pull might not exceed  $3.5\text{--}4.5 \times 10^{12} \text{ N m}^{-1}$ . This value is very similar to the estimates of ridge push  $F_{RP} = 3\text{--}3.5 \times 10^{12} \text{ N m}^{-1}$  [Turcotte and Schubert, 1982], and, although speculative, could account for the near neutral torque on plate margins, which is a basic tenet of plate tectonics theory [Chapple and Tullis, 1977; Forsyth and Uyeda, 1975].

[48] Stress transmission is effective also if plate thinning occurs. In fact a thinning of few kms, which is an average of our models', might result in a substantial drop in flexural parameters, up to several orders of magnitude, compatible with what has been estimated by oceanic forebulge inversion [Billen and Gurnis, 2005], yet may not significantly affect slab pull transmission.

[49] Large-scale models, where numerical resolution in the lithosphere might be too low to capture the bending process, usually display limited stress propagation and large deformation, i.e., low plate-ness [Bercovici, 2002; Tackley, 1998]. Furthermore when a constant viscosity profile is used to repre-

sent plates, the misfit of global plate motions and stress field in the convergent margin is significant [Becker and O'Connell, 2001; Conrad and Lithgow-Bertelloni, 2002; Steinberger et al., 2001], thus suggesting that the bending properties of plates play an important role in global tectonics.

## 6. Conclusions

[50] We investigated the dynamics of the bending at trench zones by analyzing dissipation and slab pull propagation in a set of fully dynamic subduction models. Our results show that the dissipation in the bend is almost independent of plate viscosity, and rather is controlled by the rate of work done by the slab pull, which is the differential of potential energy and mantle dissipation. Curvature radii and dips adjust according the mechanical properties of the plates so that a similar bending dissipation is attained in different rheological models. A comparison with a compilation of data from natural subduction zones shows that slab radii and dips on Earth readjust following an anticorrelated trend similar to that found in our models. In the models, large pull propagation is possible only if strong cores guide stresses through the bending area, allowing the transmission of 70 – 80% of the slab pull. Our results show that in plates with a strong core, bending dissipation is low, yet this does not imply that plates are too weak for the propagation of pull forces from deep slabs. This suggests that plates on Earth that weakly resist bending still allow large forces to be transmitted to plates at surface.

## Acknowledgments

[51] We are grateful to D. May, C. Faccenna, L. Moresi, and D. Stegman for helpful discussions. The careful reviews of C. Conrad and an anonymous reviewer contributed to the improvement of the paper. This research was supported under Australian Research Council's Discovery Projects funding scheme (projects DP0663258 and DP0878501). Part of this work was funded by a Swiss National Fund Assistenzprofessur to S.G.

## References

Becker, T. W., and R. J. O'Connell (2001), Predicting plate velocities with mantle circulation models, *Geochem. Geophys. Geosyst.*, 2(12), 1060, doi:10.1029/2001GC000171.  
 Becker, T. W., C. Faccenna, R. J. O'Connell, and D. Giardini (1999), The development of slabs in the upper mantle: Insights from numerical and laboratory experiments, *J. Geophys. Res.*, 104, 15,207–15,226, doi:10.1029/1999JB900140.  
 Bellahsen, N., C. Faccenna, and F. Funiciello (2005), Dynamics of subduction and plate motion in laboratory experiments:

Insights into the “plate tectonics” behavior of the Earth, *J. Geophys. Res.*, 110, B01401, doi:10.1029/2004JB002999.  
 Bercovici, D. (2002), The generation of plate tectonics from mantle convection, *Earth Planet. Sci. Lett.*, 2005, 107–121.  
 Billen, M., and M. Gurnis (2005), Constraints on subducting plate strength within the Kermadec trench, *J. Geophys. Res.*, 110, B05407, doi:10.1029/2004JB003308.  
 Billen, M., and G. Hirt (2007), Rheologic controls on slab dynamics, *Geochem. Geophys. Geosyst.*, 8, Q08012, doi:10.1029/2007GC001597.  
 Buckmaster, J. D., A. Nachman, and L. Ting (1975), Buckling and stretching of a viscida, *J. Fluid Mech.*, 69, 1–20, doi:10.1017/S0022112075001279.  
 Buffett, B. A. (2006), Plate force due to bending at subduction zones, *J. Geophys. Res.*, 111, B09405, doi:10.1029/2006JB004295.  
 Buffett, B. A., and D. B. Rowley (2006), Plate bending at subduction zones: Consequences for the direction of plate motions, *Earth Planet. Sci. Lett.*, 245, 359–364, doi:10.1016/j.epsl.2006.03.011.  
 Capitanio, F. A., G. Morra, and S. Goes (2007), Dynamic models of downgoing plate-buoyancy driven subduction: Subduction motions and energy dissipation, *Earth Planet. Sci. Lett.*, 262, 284–297, doi:10.1016/j.epsl.2007.07.039.  
 Chapple, W. M., and T. E. Tullis (1977), Evaluation of forces that drive plates, *J. Geophys. Res.*, 82(14), 1967–1984, doi:10.1029/JB082i014p01967.  
 Cloos, M. (1993), Lithospheric buoyancy and collisional orogenesis: Subduction of oceanic plateaus, continental margins, island arcs, spreading ridges, and seamounts, *Geol. Soc. Am. Bull.*, 105, 715–737, doi:10.1130/0016-7606(1993)105<0715:LBACOS>2.3.CO;2.  
 Conrad, C. P., and B. H. Hager (1999), Effects of plate bending and fault strength at subduction zones on plate dynamics, *J. Geophys. Res.*, 104, 17,551–17,571, doi:10.1029/1999JB900149.  
 Conrad, C. P., and B. H. Hager (2001), Mantle convection with strong subduction zones, *Geophys. J. Int.*, 144, 271–288, doi:10.1046/j.1365-246x.2001.00321.x.  
 Conrad, C. P., and C. Lithgow-Bertelloni (2002), How mantle slabs drive plate tectonics, *Science*, 298, 207–209, doi:10.1126/science.1074161.  
 Conrad, C. P., and C. Lithgow-Bertelloni (2004), The temporal evolution of plate driving forces: Importance of “slab suction” versus “slab pull” during the Cenozoic, *J. Geophys. Res.*, 109, B10407, doi:10.1029/2004JB002991.  
 Conrad, C. P., S. Bilek, and C. Lithgow-Bertelloni (2004), Great earthquakes and slab pull: Interaction between seismic coupling and plate-slab coupling, *Earth Planet. Sci. Lett.*, 218, 109–122, doi:10.1016/S0012-821X(03)00643-5.  
 Di Giuseppe, E., J. van Hunen, F. Funiciello, C. Faccenna, and D. Giardini (2008), Slab stiffness control of trench motion: Insights from numerical models, *Geochem. Geophys. Geosyst.*, 9, Q02014, doi:10.1029/2007GC001776.  
 Elsasser, W. M. (1969), Convection and stress propagation in the upper mantle, in *The Application of Modern Physics to the Earth and Planetary Interiors*, edited by S.K. Runcorn, pp. 223–249, John Wiley, New York.  
 Enns, A., T. W. Becker, and H. Schmeling (2005), The dynamics of subduction and trench migration for viscosity stratification, *Geophys. J. Int.*, 160, 761–769, doi:10.1111/j.1365-246X.2005.02519.x.  
 Faccenna, C., A. Heuret, F. Funiciello, S. Lallemand, and T. W. Becker (2007), Predicting trench and plate motion from the dynamics of a strong slab, *Earth Planet. Sci. Lett.*, 257, 29–36, doi:10.1016/j.epsl.2007.02.016.



- Forsyth, D., and S. Uyeda (1975), On the relative importance of driving forces of plate motion, *Geophys. J. R. Astron. Soc.*, *43*, 163–200.
- Funiciello, F., G. Morra, K. Regenauer-Lieb, and D. Giardini (2003), Dynamics of retreating slabs: 1. Insights from two-dimensional numerical experiments, *J. Geophys. Res.*, *108*(B4), 2206, doi:10.1029/2001JB000898.
- Funiciello, F., C. Faccenna, A. Heuret, S. Lallemand, E. Di Giuseppe, and T. W. Becker (2008), Trench migration, net rotation and slab-mantle coupling, *Earth Planet. Sci. Lett.*, *271*, 233–240, doi:10.1016/j.epsl.2008.1004.1006.
- Goes, S., F. Capitanio, and G. Morra (2008), Evidence of lower mantle slab penetration phases in plate motions, *Nature*, *451*, 981–984, doi:10.1038/nature06691.
- Goetze, C., and B. Evans (1979), Stress and temperature in the bending lithosphere as constrained by experimental rock mechanics, *Geophys. J. R. Astron. Soc.*, *59*, 463–478.
- Hibbit, Karlsson, and Soerenson Inc. (1999), ABAQUS user manual, Providence, R.I.
- Kameyama, M., D. A. Yuen, and S.-I. Karato (1999), Thermal-mechanical effects of low-temperature plasticity (the Peierls mechanism) on the deformation of a viscoelastic shear zone, *Earth Planet. Sci. Lett.*, *168*, 159–172, doi:10.1016/S0012-821X(99)00040-0.
- Karato, S. I., and P. Wu (1993), Rheology of the upper mantle—A synthesis, *Science*, *260*, 771–778, doi:10.1126/science.260.5109.771.
- Kohlstedt, D. L., B. Evans, and S. J. Mackwell (1995), Strength of the lithosphere: Constraints imposed by laboratory experiments, *J. Geophys. Res.*, *100*, 17,587–17,602, doi:10.1029/95JB01460.
- Lallemand, S., A. Heuret, and D. Boutelier (2005), On the relationships between slab dip, back-arc stress, upper plate absolute motion, and crustal nature in subduction zones, *Geochem. Geophys. Geosyst.*, *6*, Q09006, doi:10.1029/2005GC000917.
- Lithgow-Bertelloni, C., and J. H. Guynn (2004), Origin of the lithospheric stress field, *J. Geophys. Res.*, *109*, B01408, doi:10.1029/2003JB002467.
- Lithgow-Bertelloni, C., and M. A. Richards (1995), Cenozoic plate driving forces, *Geophys. Res. Lett.*, *22*, 1317–1320, doi:10.1029/95GL01325.
- Lithgow-Bertelloni, C., and M. A. Richards (1998), The dynamics of Cenozoic and Mesozoic plate motions, *Rev. Geophys.*, *36*, 27–78, doi:10.1029/97RG02282.
- Mitrovica, J. X. (1996), Haskell [1935] revisited, *J. Geophys. Res.*, *101*, 555–569, doi:10.1029/95JB03208.
- Moresi, L., and M. Gurnis (1996), Constraints on the lateral strength of slabs from three-dimensional dynamic flow models, *Earth Planet. Sci. Lett.*, *138*, 15–28, doi:10.1016/0012-821X(95)00221-W.
- Morra, G., and K. Regenauer-Lieb (2006a), A coupled solid-fluid method for modeling subduction, *Philos. Mag.*, *86*, 3307–3323, doi:10.1080/14786430500256359.
- Morra, G., and K. Regenauer-Lieb (2006b), On the Curvature of Oceanic Arcs, *Geology*, *34*, 877–880, doi:10.1130/G22462.1.
- Ranalli, G. (1987), *Rheology of the Earth*, Chapman and Hall, London.
- Regenauer-Lieb, K., B. Hobbs, D. A. Yuen, A. Ord, Y. Zhang, H. B. Mulhaus, and G. Morra (2006a), From point defects to plate tectonic faults, *Philos. Mag.*, *86*, 3373–3392, doi:10.1080/14786430500375159.
- Regenauer-Lieb, K., R. F. Weinberg, and G. Rosenbaum (2006b), The effect of energy feedbacks on continental strength, *Nature*, *442*, 67–70, doi:10.1038/nature04868.
- Ribe, N. M. (2001), Bending and stretching of thin viscous sheets, *J. Fluid Mech.*, *433*, 135–160.
- Royden, L. H. (1993), The tectonic expression of slab pull at continental convergent boundaries, *Tectonics*, *12*, 303–325, doi:10.1029/92TC02248.
- Schellart, W. P. (2004a), Kinematics of subduction and subduction-induced flow in the upper mantle, *J. Geophys. Res.*, *109*, B07401, doi:10.1029/2004JB002970.
- Schellart, W. P. (2004b), Quantifying the net slab pull force as a driving mechanism for plate tectonics, *Geophys. Res. Lett.*, *31*, L07611, doi:10.1029/2004GL019528.
- Schellart, W. P. (2008), Kinematics and flow patterns in deep mantle and upper mantle subduction models: Influence of the mantle depth and slab to mantle viscosity ratio, *Geochem. Geophys. Geosyst.*, *9*, Q03014, doi:10.1029/2007GC001656.
- Stegman, D. R., J. Freeman, W. P. Schellart, L. Moresi, and D. May (2006), Influence of trench width on subduction hinge retreat rates in 3-D models of slab rollback, *Geochem. Geophys. Geosyst.*, *7*, Q03012, doi:10.1029/2005GC001056.
- Stein, C. A., and S. Stein (1992), A model for the global variation in oceanic depth and heat flow with lithospheric age, *Nature*, *359*, 123–129, doi:10.1038/359123a0.
- Steinberger, B., H. Schmeling, and G. Marquart (2001), Large-scale lithospheric stress field and topography induced by global mantle circulation, *Earth Planet. Sci. Lett.*, *186*, 75–91, doi:10.1016/S0012-821X(01)00229-1.
- Tackley, P. J. (1998), Self-consistent generation of tectonic plates in three-dimensional mantle convection, *Earth Planet. Sci. Lett.*, *157*, 9–22, doi:10.1016/S0012-821X(98)00029-6.
- Turcotte, D. L., and G. Schubert (1982), *Geodynamics, Application of Continuum Mechanics to Geological Problems*, John Wiley, New York.
- Turcotte, D. L., D. C. McAdoo, and J. G. Caldwell (1978), An elastic-perfectly plastic analysis of the bending of the lithosphere at the trench, *Tectonophysics*, *47*, 193–205, doi:10.1016/0040-1951(78)90030-6.
- Wu, B., C. P. Conrad, A. Heuret, C. Lithgow-Bertelloni, and S. Lallemand (2008), Reconciling strong slab pull and weak plate bending: The plate motion constraint on the strength of mantle slabs, *Earth Planet. Sci. Lett.*, *272*, 412–421.
- Zhong, S., and G. F. Davies (1999), Effects of plate and slab viscosities on the geoid, *Earth Planet. Sci. Lett.*, *170*, 487–496, doi:10.1016/S0012-821X(99)00124-7.